

DETC2021-67573

OPEN-LOOP CONTROL CO-DESIGN OF FLOATING OFFSHORE WIND TURBINES USING LINEAR PARAMETER-VARYING MODELS

Athul K. Sundarrajan¹, Yong Hoon Lee², James T. Allison², Daniel R. Herber^{1*}

¹Department of Systems Engineering
Colorado State University
Fort Collins, CO 80523

²Department of Industrial and Enterprise Systems Engineering
University of Illinois at Urbana-Champaign
Urbana, IL 61801

ABSTRACT

This paper discusses a framework to design elements of the plant and control systems for floating offshore wind turbines (FOWTs) in an integrated manner using linear parameter-varying models. Multiple linearized models derived from high-fidelity software are used to model the system in different operating regions characterized by the incoming wind speed. The combined model is then used to generate open-loop optimal control trajectories as part of a nested control co-design strategy that explores the system's stability and power production in the context of crucial plant and control design decisions. A cost model is developed for the FOWT system, and the effect of plant decisions and subsequent power and stability response of the FOWT is quantified in terms of the levelized cost of energy (LCOE) for that system. The results show that the stability constraints and the plant design decisions affect the turbine's power and, subsequently, LCOE of the system. The results indicate that a lighter plant in terms of mass can produce the same power for a lower LCOE while still satisfying the constraints.

Keywords: floating offshore wind turbines; linear parameter-varying models; control co-design; optimal control; levelized cost of energy

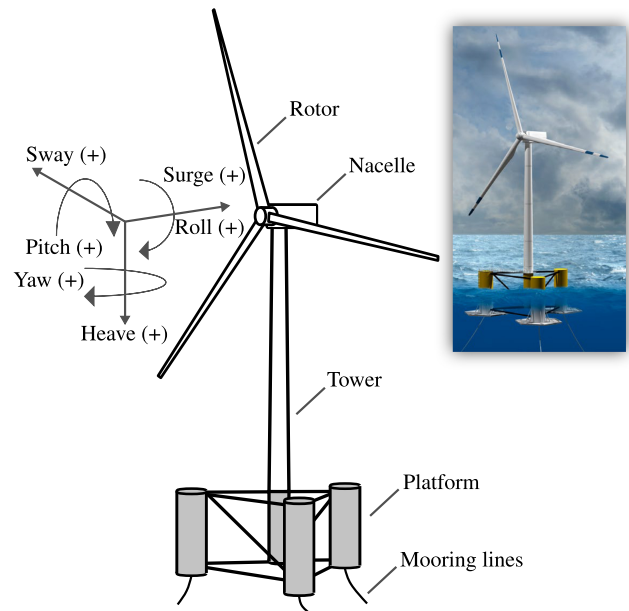


FIGURE 1: Floating offshore wind turbine (illustration courtesy of NREL).

1 INTRODUCTION

The design of floating offshore wind turbines (FOWTs) has often followed a sequential pattern, where the physical plant pa-

*Corresponding author, daniel.herber@colostate.edu

rameters are designed first, and a controller is then optimized for this particular plant [1–4]. However, in FOWTs, there are strong interactions between the structural and environmental dynamics and the controller. Unfortunately, a sequential design process can produce unstable systems as it does not account for this coupling [5, 6]. Optimizing both the physical plant and the controller simultaneously enables rapid identification of stable, system-level optimal results. This integrated design approach has been studied extensively under the term control co-design (CCD) [1, 7–11]. Recently the importance of these integrated design approaches for energy system design has been recognized by domain experts. References [5, 12, 13] have explored the application of integrated design to offshore wind turbines, and Refs. [14, 15] discuss the application of CCD to the design of wave energy systems. Integrated design approaches have also found applications in design of mixed renewable/nonrenewable power generation systems [16].

The primary design goal of any wind-based energy system is to capture as much power from the incoming wind while minimizing the structure’s dynamic loads. However, the overarching balance between increasing the annual energy production while minimizing the systems’ building and operating costs is essential to producing economical energy solutions. These goals are captured by the levelized cost of energy (LCOE) [17]:

$$\text{LCOE} = \frac{\text{Total Lifetime Cost}}{\text{Total Lifetime Energy Output}} \quad (1)$$

The total lifetime costs of the FOWT system are a combination of the initial cost needed to build the system (capital cost) and the maintenance costs over its lifetime. The capital costs are often directly linked to some of the plant design decisions [18, 19]. The maintenance costs and the total lifetime energy output are dependent on how the system operates and, consequently, depend on the environment and how it is controlled [20]. Recent studies have shown that advanced control strategies for offshore wind applications can increase the power extracted from the turbine and minimize the levelized cost [21]. Most conventional LCOE estimates have not incorporated detailed dynamic assessments nor the impact of novel control strategies. In the case of highly-coupled, highly-constrained systems like FOWTs, such considerations are imperative because of the many challenges making these systems economically viable [22]. Additionally, overlooking the impacts of control decisions on the optimal physical design is a pitfall of sequential design approaches.

1.1 Plant Design of Floating Offshore Wind Turbines

The plant design of a FOWT involves design decisions for several individual subsystems and considerations of stability, cost, and energy production. The primary elements of a FOWT are the rotor, drivetrain, nacelle, tower, and support structure, and are labeled in Fig. 1.

Stability of the FOWT about its natural equilibrium is re-

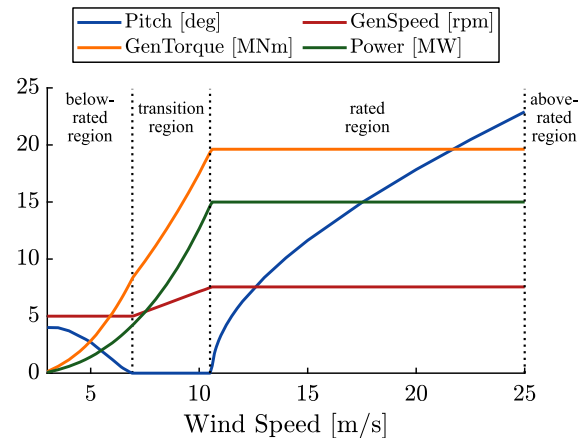


FIGURE 2: Controller regulation trajectories from Ref. [12].

quired in all manner of wind, wave, and current excitations that the system might experience [23]. Reference [24] provides information about the current standard industry requirements of a FOWT. Generally, increasing the mass of the support structure will make the FOWT more stable, but this would also raise the capital and other costs. Therefore, it is essential to optimize the system for cost while ensuring stability [25]. As the development cycle progresses, additional practical considerations like assembly costs and procedures, maintenance costs, and ease of transportation may also be incorporated into the plant design.

1.2 Wind Turbine Control of Floating Offshore Wind Turbines

The control system for a FOWT is instrumental in achieving the design goals stated in the previous sections. The power generated by a FOWT and the physical loads on its structure is heavily dependent on the loading conditions induced by the wind, waves, and currents. Operating the system in such a way so that it can remain stable while producing maximal power is the primary goal of the FOWT control system. Similar to the control of land-based wind turbines, the control strategy selected depends heavily on the system’s input excitations, as these inputs produce the dynamical responses we seek to optimize.

The primary mode of control for any wind turbine depends heavily on the wind, so specific operating regions are often defined based on the wind speed [26, 27]. Typically, there are four wind speed-based regions of interest, visualized in Fig. 2. At the lower, below-rated wind speeds, the system produces limited power. Above the rated wind speed, the turbine is designed to operate at its maximum power level. In between these regions, there is a transition behavior, and at extremely fast, above-rated wind speeds, the system is shut down as there can be permanent structural damage.

The two primary control inputs for wind turbines are the

pitch angle of the turbine blades (commonly called blade pitch) and the torque produced by the generator. In below-rated wind speeds, varying the generator torque is the primary mode of control of the turbine [12]. At rated wind speeds, the generator torque is held constant, and the blade pitch is varied in a process called maximum power point tracking, where the rotor's angular velocity is continuously adjusted to extract the maximum possible power from the incoming wind.

1.3 Modeling Considerations

It is often necessary to conduct early-stage design studies to understand the desired fundamental system properties and behaviors that inform critical decisions that need to be made as the system-of-interest is realized. The use of high-fidelity modeling tools in early-stage design studies is not always needed to achieve the desired design insights and can be prohibitive due to their complexity and computational expense.

To facilitate these design and control (both closed- and open-loop) studies, it is common to develop reduced or lower-order models that capture just the system's essential physics. Results from these reduced-order models are validated against the simulations from high-fidelity tools to understand their veracity in studying the system's behavior. After validation, these models are then linearized around predetermined set-point values in distinct operating regions. These linearized models are then used to understand the system dynamics and design controllers in these operating regions. However, there are some drawbacks to developing these lower-order models. The development of these lower-order models is complicated as they require extensive subject knowledge of FOWTs and the associated physics/engineering disciplines. Additionally, the lower-order models are developed to study a specific aspect of the system's behavior, e.g., the floating structure response, controller response, aerodynamic wake, etc. As such, the results from these models cannot be easily generalized. The highly-coupled nature of a FOWT can create further complications in modeling the system accurately [5, 28–31].

One way to mitigate these difficulties is by using linearized models obtained directly from high-fidelity (e.g., computational fluid dynamics) modeling tools [32, 33]. These models are obtained by linearizing the nonlinear system around specific operating points, often stationary points where the system exhibits static behavior. A linear time-invariant state-space dynamic model about the static operating point (ξ_o, u_o) typically has the following form:

$$\frac{d\xi_{\Delta}(t)}{dt} = A_o \xi_{\Delta}(t) + B_o u_{\Delta}(t) \quad (2a)$$

$$y(t) = C_o \xi_{\Delta}(t) + D_o u_{\Delta}(t) + g_o \quad (2b)$$

where t is time, $\xi_{\Delta}(t)$ are the relative states related to the original states ξ with $\xi(t) = \xi_{\Delta}(t) + \xi_o$, $u_{\Delta}(t)$ are the relative inputs related to the original inputs u with $u(t) = u_{\Delta}(t) + u_o$, $y(t)$ are

the outputs, and the matrices $(A_o, B_o, C_o, D_o, g_o)$ are associated with the linearization process.

A significant drawback with any kind of linearized model is their accuracy in capturing the system's dynamic response diminishes quickly as the system's behavior moves away from the initial operating point. Thus, it becomes difficult to work with many diverse design load cases, where the wind speed continuously varies. Some studies that have used linearized models have leveraged them in gain scheduling approaches to account for nonlinearities. However, this approach does not guarantee stability and performance for all possible values of the wind speed [34].

In this work, we will discuss the use of linear parameter-varying (LPV) models to help overcome the drawbacks of distinct linear models [34, 35]. These LPV models show good accuracy when capturing the original nonlinear dynamics and can be used to generate open-loop optimal control trajectories. Additionally, LPV models have been used to develop closed-loop controllers for wind turbines [34, 36].

1.4 Integrated Design with Control Co-Design

CCD is an integrated design paradigm that enables simultaneous design optimization of the plant and control systems [10, 37–39]. The CCD approach provides a rigorous framework that can naturally handle the coupling between the plant and control drivers present in FOWTs. A common mathematically-equivalent way to decompose a CCD problem is with the nested formulation and bilevel optimization [37, 38]. The coordination approach defines a first-level, outer-loop problem that optimizes the plant design with information on the best possible performance from the second-level, inner-loop problem that optimizes the dynamics and control for a given plant design (and is sometimes called the control subproblem). In other words, the outer loop generates candidate plant designs x_p^{\dagger} ; this candidate is then passed to the inner loop. The inner loop then produces an optimal control solution x_c and system dynamic states ξ for this candidate plant design.

There are certain advantages in using the nested CCD approach (many are discussed in Ref. [38]), especially for problems where the inner loop is a linear-quadratic dynamic optimization (LQDO) problem. LQDO problems are characterized by quadratic objectives, linear dynamic systems, general linear constraints, and open-loop control [38, 40]. Such problems can be solved efficiently and accurately using quadratic programming methods [41]. The use of open-loop control during early-stage design studies can show the maximum achievable performance of the system and provide the desired insights into the optimal system dynamics and controller behavior [14, 38, 42]. Additionally, nested CCD is often necessary when black-box models of the dynamics are used (as will be the case in this work) [8, 43].

1.5 Use of OpenFAST and WEIS Models

The wind energy with integrated servo-control (WEIS) is an open-source project that is currently being developed by the National Renewable Energy Laboratory (NREL) and partners that will allow users to perform CCD of FOWT systems [2, 44]. The WEIS toolbox is built on OpenFAST, another open-source toolbox developed by NREL, that generates a full-system dynamic response of FOWTs under wind, wave, and current excitations. The OpenFAST tool is built on independent modules that capture the important physical phenomena of the different FOWT subsystems and couplings between them. There are different modules to capture the effects of aerodynamics, hydrodynamics, servodynamics, and mooring dynamics. A variety of plant design decisions can be explored within these tools as well [2].

In this work, the dynamic models of FOWTs will be generated using the linearization capabilities of the WEIS/OpenFAST tools, with the original nonlinear dynamics simulation capabilities being used for validation of the results. A detailed discussion regarding the linearization capabilities of OpenFAST and the entire tool can be found in Refs. [32, 33, 44, 45]. Wind speed is used to select the state and control operating points for this linearized model.

The remainder of the paper is organized as follows. Sections 2 and 3 define LPV modeling theory and validates the specific LPV models used in this work, respectively. Section 4 formulates the CCD problem using the LPV dynamic model. Section 5 presents the results of several studies conducted to better understand the impact of control and plant decisions on the LCOE objective. Section 6 summarizes the results and provides future steps for this work.

2 LINEAR PARAMETER-VARYING MODELS

As mentioned in Sec. 1.3, linearized models, like the one defined in Eq. (2), can accurately describe the system's behavior for small perturbations about the operating point from which they were derived. For the design and optimization activities of a FOWT system, it is essential to understand the system behavior over multiple input excitations. While there are additional drivers for modeling variations, the primary one in wind energy systems, including FOWTs, is the wind speed in the direction of the turbine-blade system. Under different wind conditions, the stationary operating points for the FOWT system greatly vary, as do the matrices defining the dynamic model in Eq. (2). Therefore, we will consider models dependent on this important parameter and will be useful in open-loop optimal control CCD studies.

2.1 Linear Parameter-Varying Model Derivation

LPV models are a special case of linear time-varying (LTV) systems where the system matrices are continuous and are a function of a set of parameters [35, 46]. Here, we will consider the single

parameter case where the parameter w indicates the current wind speed value. Now, consider the following nonlinear parameter-dependent model Σ :

$$\Sigma = \begin{cases} \frac{d\xi}{dt} = \mathbf{f}(\xi, \mathbf{u}, w) \\ \mathbf{y} = \mathbf{g}(\xi, \mathbf{u}, w) \end{cases} \quad (3)$$

Our goal is to linearize this model about the w -varying operating point functions $(\xi_o(w), \mathbf{u}_o(w))$ where stationary or steady-state models characterize their values:

$$\mathbf{f}(\xi_o(w), \mathbf{u}_o(w), w) = \mathbf{0}, \quad \forall w \in [w_{\min}, w_{\max}] \quad (4)$$

where w_{\min} is the minimum parameter value considered and w_{\max} the maximum.

Now, the relationship between the linearization states and the original states depends on the parameter w :

$$\xi(t) = \xi_{\Delta}(t) + \xi_o(w), \quad \mathbf{u}(t) = \mathbf{u}_{\Delta}(t) + \mathbf{u}_o(w) \quad (5)$$

Assuming that w is time varying, the time derivative relationship of the states is:

$$\frac{d\xi}{dt} = \frac{d\xi_{\Delta}}{dt} + \frac{d}{dt}\xi_o(w(t)) \quad (6a)$$

$$= \frac{d\xi_{\Delta}}{dt} + \frac{\partial \xi_o}{\partial w} \frac{dw}{dt} \quad (6b)$$

Now, we use the following notation for the derivatives of the nonlinear model:

$$\mathbf{A}(w) := \mathbf{J}_{\xi}^{\mathbf{f}}(\xi_o(w), \mathbf{u}_o(w), w), \quad \mathbf{B}(w) := \mathbf{J}_{\mathbf{u}}^{\mathbf{f}}(\xi_o(w), \mathbf{u}_o(w), w)$$

$$\mathbf{C}(w) := \mathbf{J}_{\xi}^{\mathbf{g}}(\xi_o(w), \mathbf{u}_o(w), w), \quad \mathbf{D}(w) := \mathbf{J}_{\mathbf{u}}^{\mathbf{g}}(\xi_o(w), \mathbf{u}_o(w), w)$$

where $\mathbf{J}_x^{\mathbf{f}}$ denotes the Jacobian of \mathbf{f} with respect to \mathbf{x} , and the values of these functions are dependent on the operating points and are denoted as:

$$\mathbf{f}(w) := \mathbf{f}(\xi_o(w), \mathbf{u}_o(w), w), \quad \mathbf{g}(w) := \mathbf{g}(\xi_o(w), \mathbf{u}_o(w), w)$$

With this derivative relationship in Eq. (6) and the notation above, the nonlinear system Σ in Eq. (3) is linearized about $(\xi_o(w), \mathbf{u}_o(w))$ yielding the following LPV system:

$$\Sigma_w = \begin{cases} \frac{d\xi_{\Delta}}{dt} = \overset{0}{\mathbf{f}(w)} + \mathbf{A}(w)\xi_{\Delta} + \mathbf{B}(w)\mathbf{u}_{\Delta} - \frac{\partial \xi_o(w)}{\partial w} \frac{dw}{dt} \\ \mathbf{y} = \mathbf{g}(w) + \mathbf{C}(w)\xi_{\Delta} + \mathbf{D}(w)\mathbf{u}_{\Delta} \end{cases} \quad (8)$$

Note, if only a single time-invariant value of the parameter denoted w_o is considered, then we have the following system:

$$\frac{d\xi_{\Delta}}{dt} = \mathbf{A}(w_o)\xi_{\Delta} + \mathbf{B}(w_o)\mathbf{u}_{\Delta} - \frac{\partial \xi_o(w_o)}{\partial w} \frac{dw}{dt} \quad (9a)$$

$$\mathbf{y} = \mathbf{g}(w_o) + \mathbf{C}(w_o)\xi_{\Delta} + \mathbf{D}(w_o)\mathbf{u}_{\Delta} \quad (9b)$$

which gives us:

$$\Sigma_o = \begin{cases} \frac{d\xi_{\Delta}}{dt} = \mathbf{A}(w_o)\xi_{\Delta} + \mathbf{B}(w_o)\mathbf{u}_{\Delta} \\ \mathbf{y} = \mathbf{g}(w_o) + \mathbf{C}(w_o)\xi_{\Delta} + \mathbf{D}(w_o)\mathbf{u}_{\Delta} \end{cases} \quad (10)$$

which is the same LTI system defined in Eq. (2) for a single operating point characterized by the parameter w_o .

2.2 Construction using Multiple Linearized Models

The system Σ_w with continuous dependence on the parameter w generally will not be directly available because linearized models are often realized through numerical methods for specific operating points (i.e., Σ_o). Therefore, it may be necessary to construct Σ_w from a finite strategic set of Σ_o models. To accomplish this goal, the matrix entries of Σ_w are determined by element-wise matrix interpolation from a set of given denoted $\Omega = \{\Sigma_{o1}, \Sigma_{o2}, \dots, \Sigma_{on}\}$ each created using the parameters values $\mathbf{W} = [w_1, w_2, \dots, w_n]$. Derivatives of the polynomial interpolating function are directly computed when needed.

Now, there are several properties to consider to ensure such an interpolation scheme has reasonable chance of meaningfully capturing the nonlinear dynamics including:

- (P1) The states, inputs, and outputs are unchanging for all considered Σ_o .
- (P2) The sparsity patterns (nonzero entries in the system matrices) are generally similar between analogous matrices.
- (P3) The stationary condition in Eq. (4) holds for the given interpolation scheme and \mathbf{W} , i.e., $(\xi_o(w), u_o(w))$ can be found through interpolation such that the condition holds.
- (P4) The element-wise relationships between different matrices can be reasonably interpolated using a selected \mathbf{W} (note that this is hard to quantify because errors in these coefficients might not result in large errors in the key outputs).
- (P5) At various validation points not in \mathbf{W} , the error between the actual linearized system at w_o and the interpolated system Σ_w quantified by the H_∞ norm is below a tolerance ϵ :

$$\|\mathbf{G}_o(s) - \mathbf{G}_w(s)\|_{H_\infty} \leq \epsilon \quad (11)$$

where $\mathbf{G}_o(s)$ and $\mathbf{G}_w(s)$ are the transfer function matrices for Σ_o and Σ_w , respectively. Note that this error metric better captures the input/output error in the system.

- (P6) Time-domain simulations between the nonlinear Σ and LPV Σ_w should be similar.

At this time, the selection of \mathbf{W} was informed by expert intuition and figures like Fig. 2 that characterize the different regions of operation and their transition points. Future work will consider automated sampling strategies that try to optimally sample points for constructing an accurate LPV using the condition in Eq. (11).

3 LPV Model Validation for IEA-15 MW Turbine

The International Energy Agency (IEA) 15 MW offshore wind turbine is a reference turbine model jointly developed by NREL and Danish Technical University (DTU) [12, 47], visualized in Fig. 1. The turbine is supported by a floating semisubmersible platform and a chain catenary mooring system. The details of the support structure are available in Ref. [48]. This is the system under consideration in this work.

Two keys states in this system are the generator speed ω_g

and platform pitch Θ_p . In its current form, the model is excited by wind inputs only; wave and current disturbances are not considered. Correspondingly, the total inputs to the system are the wind speed w , the generator torque τ_g , and the blade pitch β :

$$\mathbf{u}(t) = \begin{bmatrix} w & \tau_g & \beta \end{bmatrix}^T \quad (12)$$

For the considered system, the OpenFAST tool can provide accurate simulations of the system's nonlinear dynamics (i.e., the outputs of Σ). However, due to the concerns expressed in the previous sections, an LPV model is considered a less computationally-expensive and structured alternative to these expensive simulations. The natural choice for the parameter needed to construct the LPV model Σ_w is the wind speed. The operating region of a wind turbine is between the cut-in wind speed ($w_{\min} = 3$ [m/s] in this study) and the cut-out wind speed ($w_{\max} = 25$ [m/s]). More points were sampled in the region between rated wind speed and below-rated wind speed to ensure accurate modeling. To understand the accuracy of the LPV modeling approach for this system, several comparisons were made.

3.1 State-Space Model Comparisons

With a selected \mathbf{W} (56 distinct wind speeds), the set of linearized state-space models Ω at each of the wind speed values are obtained. To construct the continuous Σ_w using \mathbf{W} and Ω , direct element-wise interpolation of the matrices ($\mathbf{A}_o, \mathbf{B}_o, \mathbf{C}_o, \mathbf{D}_o$) was used. To reduce the interpolation costs, matrix sparsity patterns were considered. Only entries with nonzero values were interpolated (and the sparsity pattern remained similar (P2)).

To understand the predictive accuracy of this approach, and check if these models satisfy (P4), the following test is carried out. Every alternate point in \mathbf{W} was chosen as a training data for the interpolation procedure, and the values in-between are selected as validation points. This allows us to assess if the interpolation approach can predict matrix properties by comparing to the validation systems¹. In Fig. 3a, several key $\xi_o(w)$ and $u_o(w)$ are shown and there is good agreement between the interpolated LPV system and the validation points, even in the transition region. In Fig. 3b, one of the eigenvalues of $\mathbf{A}(w)$ that changes with the wind is shown. Again, the eigenvalues generally are well predicted with the largest errors in the transition region. Finally, the normalized nonzero entries of $\mathbf{B}(w)$ are shown in Fig. 3c. There are some validation points with high error in the transition region but good agreement in the other regions.

3.2 Frequency-Domain Verification

The transfer function matrix of the LPV models was studied to understand better if the input/output relationship is accurately predicted and compute the error in Eq. (11) in (P5). Here, we consider the six relationships between the two key states (ω_g and Θ_p) and the inputs \mathbf{u} .

¹All points in \mathbf{W} are used in the studies in Sec. 5.

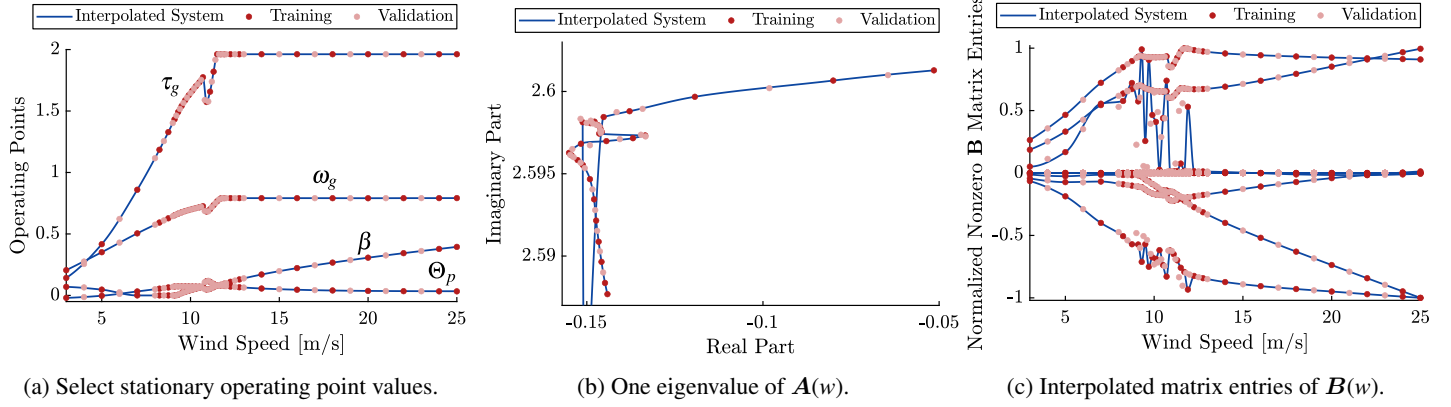


FIGURE 3: Select stationary points, eigenvalues, and input matrix for Σ_w for the IEA-15.

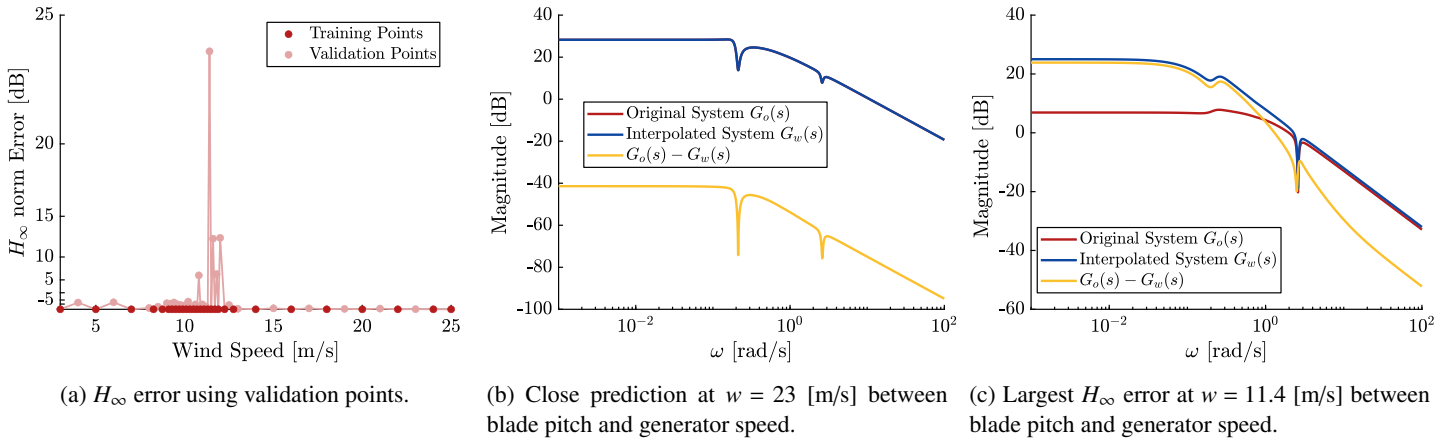


FIGURE 4: Transfer function-based comparisons using the validation wind speed values for the IEA-15.

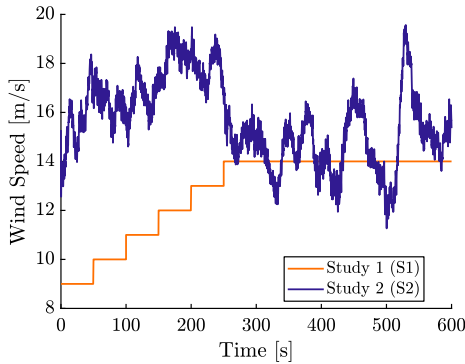


FIGURE 5: Two different wind inputs used in the Time-Domain Verification simulations.

The H_∞ norm error between the training and validation systems and the interpolated systems is shown in Fig. 4a. The errors

at the training points are near zero, as expected using interpolation. However, the systems derived from the transition region (8–12 [m/s]) have the highest error compared to the other regions. This figure shows how advanced sampling strategies could be used to better sample from regions of high error. Additionally, the transfer functions between β and ω_g are shown in Figs. 4b and 4c with a close prediction and largest H_∞ error, respectively.

3.3 Time-Domain Verification

The final comparisons were based on (P6) using OpenFAST to determine the nonlinear response of Σ . Using the same input trajectories, three different models (Σ , Σ_w , and Σ_o using the average wind speed w_{avg}) are simulated, and then the resulting state trajectories are compared. Two different input sets were simulated. The wind inputs (step-like and turbulent) are shown in Fig. 5 (and the nonzero trajectories for β and τ_f are not shown).

From the results, we see that Σ_w captures the nonlinear response from OpenFAST more accurately than Σ_o using w_{avg} . In the first study (S1), $w_{avg} = 12.8$ [m/s]. Early in the simulation,

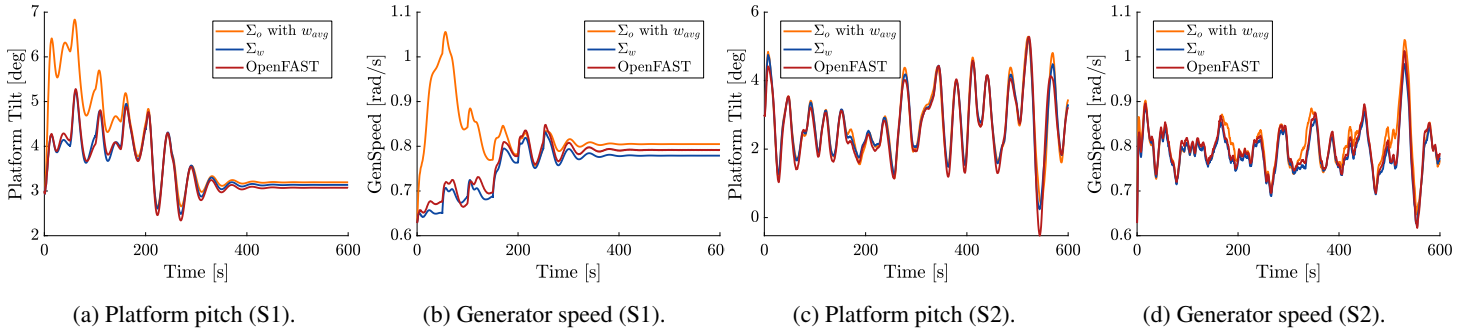


FIGURE 6: Model validation simulations between nonlinear Σ , LPV Σ_w , and LTI Σ_o using w_{avg} models.

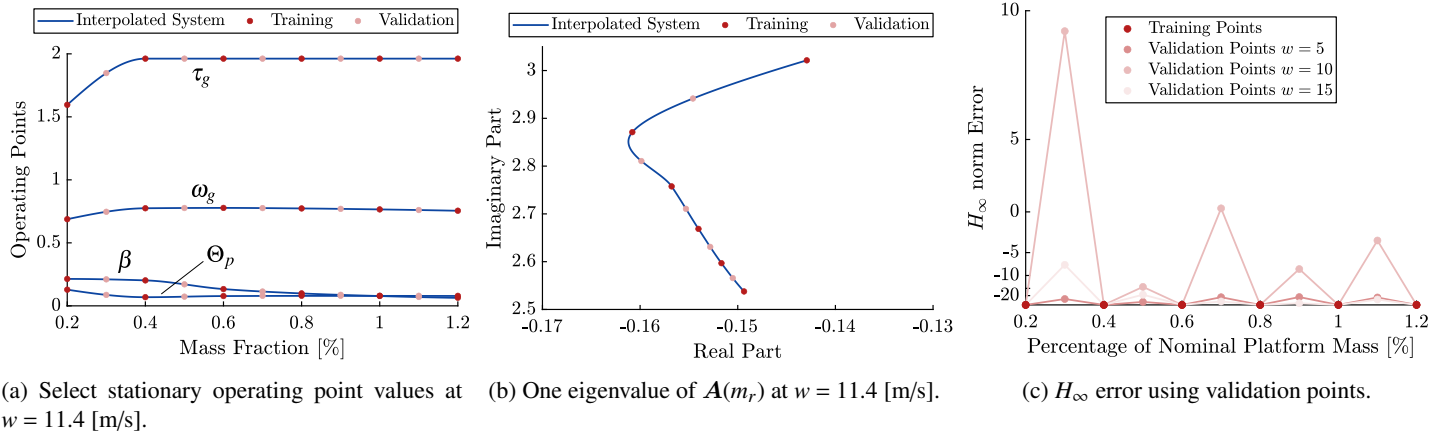


FIGURE 7: Select stationary points, eigenvalues, and H_∞ error for all eleven m_r for the IEA-15.

when the wind speed value is far away from w_{avg} , we see that the Σ_o using w_{avg} produces inaccurate results for Θ_p in Fig. 6a and ω_g in Fig. 6b. In the second study (S2), $w_{avg} = 15.7$ [m/s], and the wind profile is generally in a region where the dynamics are more predictable between wind speeds (cf. Figs. 3 and 4). Because of this property, all the model responses are similar, but again Σ_w more closely follows Σ . The simulation results for Θ_p and ω_g are in Figs. 6c and 6d, respectively.

Using all the different comparisons, it was concluded that the LPV model Σ_w can with reasonable accuracy, capture the dynamics of the considered FOWT.

3.4 Interpolation Based on Platform Mass

The model Σ_w just presented was obtained using a particular instance of the system's plant design, denoted by x_p in Sec. 1.1. However, we also want to consider the design impacts of a single plant design parameter, namely the platform mass. For such an investigation, using a collection of various values of the platform mass M , a full set of linear models Ω corresponding to W are obtained. A similar interpolation scheme and analysis are carried out in this additional dimension.

Similar tests to the ones outlined in the previous sections were carried out to check the predictive accuracy of interpolation based on the platform's mass. Denoting the nominal platform mass as $m_r = 1$, a total of eleven mass value fractions between 0.2 and 1.2 were used in this study. The nominal platform specifications are available at Ref. [48]. Stationary operating points, eigenvalues of $A(w)$ for $w = 11.5$ [m/s], and the H_∞ norm error between the training and validation mass points for wind speeds in the three different regions are shown in Fig. 7. From these results, we see that interpolation based on M is generally well behaved, potentially more so than the wind speed dimension.

4 CONTROL CO-DESIGN PROBLEM FORMULATION

This section describes the nested CCD problem constructed using the LPV models from Sec. 2 to study the impact of various stability constraints on the LCOE for the considered single device FOWT.

4.1 Outer-Loop Plant Design Problem Formulation

The outer-loop plant optimization problem in the nested CCD approach employed here is centered around the LCOE calculation in Eq. (1). In this calculation, the total lifetime cost is estimated as follows:

$$C_n = \frac{I(\mathbf{x}_p)}{(1+r)} + \sum_{k=1}^n \frac{O}{(1+r)^k} \quad (13)$$

where $I(\mathbf{x}_p)$ is the investment cost that depends on the plant design, O are the annual operating costs, r is the annual discount rate, and n is the expected lifetime of the system in years. For this study, we created a low-fidelity cost and scaling model for the blades, generator, nacelle, and tower from Refs. [49–52].

Here, we will be considering platform mass as the key plant design variable. Different platform studies use different cost models, and these cost models depend on the cost per tonne of the materials used to construct the platform. The IEA-15 turbine used in this study is a semisubmersible platform. The constituent materials used for constructing the platform are steel, fixed ballast, and outfitting, and their nominal masses and costs per tonne are from Ref. [48]. The cost of the platform relative to the nominal platform design is:

$$C_{\text{platform}} = m_r C_{\text{nominal}} \quad (14)$$

where m_r is a unitless ratio between the platform's mass and the nominal platform mass and $C_{\text{nominal}} = 15.4$ MM\$.

The total lifetime energy output is determined using a representative year long energy production calculation using m operational scenarios:

$$E = \sum_{k=1}^m \tau_k \bar{P}_k^*(w(t), \mathbf{x}_p) \quad (15)$$

where k is the operational scenario, $\bar{P}_k^*(\cdot)$ is the power, and τ_k is the expected time that the operational scenario occurs over one year. The expected average power for scenario k is determined by optimizing the dynamics and control for the given plant design and wind input. This control-focused subproblem of the nested CCD coordination strategy will be defined in the next section.

Finally, the annual energy production (AEP) is computed with:

$$\text{AEP} = \eta_u E \quad (16)$$

where $0 \leq \eta_u \leq 1$ is the expected uptime ratio. Then the expected total energy output over n years is:

$$E_n = \sum_{k=1}^n \frac{\text{AEP}}{(1+r)^k} \quad (17)$$

Therefore, $\text{LCOE} = C_n/E_n$, and the complete outer-loop optimization problem is:

$$\min_{\mathbf{x}_p} \text{LCOE}(\mathbf{x}_p) \quad (18a)$$

$$\text{subject to: } \mathbf{L}_p \leq \mathbf{x}_p \leq \mathbf{U}_p \quad (18b)$$

where only simple upper and lower bounds on the plant variables

are considered at this time (although more complex plant-only constraints can be readily incorporated).

Note that for a fixed plant, the solution for each $\bar{P}_k^*(\mathbf{x}_p)$ can be determined through independent minimization problems. Therefore, the control subproblems can be solved in parallel, reducing computational costs.

4.2 Control Subproblem for a Specific Design Load Case

The control subproblem's goal is to understand the impact of the control decisions on system response, power production, and ultimately the LCOE design objective. An open-loop optimal control problem is constructed to maximize the power produced for a given operational scenario or design load case (DLC). The optimization formulation is presented using the original (ξ, \mathbf{u}) , but the linear time-varying transformation in Eq. (5) based on the wind-dependent operating point is applied so that $(\xi_\Delta, \mathbf{u}_\Delta)$ are the states and controls for this subproblem.

The energy produced by the turbine is:

$$\int_0^{t_f} P(t) dt = \int_0^{t_f} \eta_g \tau_g(t) \omega_g(t) dt \quad (19)$$

where η_g is the generator efficiency. Note, the control term τ_g appears linearly in the objective term Eq. (19). The presence of linear control terms in the objective function with linear dynamics can give rise to singular arcs [53] as the control trajectory cannot be uniquely determined. To help mitigate this issue, a quadratic penalty term is introduced in the objective term:

$$\Pi(t) = \mathbf{u}^T \begin{bmatrix} 10^{-8} & 0 \\ 0 & 10^8 \end{bmatrix} \mathbf{u} \quad (20)$$

where values in this penalty matrix were identified according to the method discussed in Ref. [15].

The linear dynamic constraints included using Σ_w from Eq. (8) are:

$$\frac{d\xi_\Delta}{dt} = \mathbf{A}(w)\xi_\Delta + \mathbf{B}(w)\mathbf{u}_\Delta - \frac{\partial \xi_o(w)}{\partial w} \frac{dw}{dt} \quad (21)$$

where the initial state values correspond to the state operating points for $w(0)$:

$$\xi(0) = \xi_o(w(0)), \text{ or equivalently } \xi_\Delta(0) = \mathbf{0} \quad (22)$$

In order to protect the generator components from excess electrical loads and the nacelle from the dynamic loads, an upper bound for generator speed ω_g is set restricting the speed to the rated speed of the turbine:

$$\omega_g(t) \leq \omega_{g,\text{max}} \quad (23)$$

To account for the stability of the FOWT system, an upper bound on the platform pitch tilt Θ_p is included:

$$\Theta_p(t) \leq \Theta_{p,\text{max}} \quad (24)$$

Maximum and minimum value constraints are placed on the controls blade pitch β and the generator torque τ_g , according to the

TABLE 1: CCD problem parameters.

Variable	Value	Units
$\omega_{g,\max}$	0.7913	[rad/s]
$\Theta_{p,\max}$	6	[deg]
P_{\max}	15	[MW]
$\tau_{g,\max}$	19.62	[MNm]
β_{\max}	0.3948	[rad]
η_g	96.55	%

values prescribed in Ref. [12] :

$$0 \leq \tau_g(t) \leq \tau_{g,\max} \quad (25a)$$

$$0 \leq \beta(t) \leq \beta_{\max} \quad (25b)$$

An additional constraint on the pitch rate is included to ensure that the rate of change of the blade pitch is within practical limits:

$$\frac{d\beta}{dt} \leq \dot{\beta}_{\max} \quad (26)$$

Another constraint is included to ensure the power generated by the turbine does not exceed the rated power. Here we approximate the nonlinear power constraint $\tau_g \omega_g \leq P_{\max}$ with the following linear path constraint:

$$\tau_g \omega_{g,\max} + \tau_{g,\max} \omega_g \leq P_{\max} + \tau_{g,\max} \omega_{g,\max} \quad (27)$$

Now, the complete control subproblem formulation is:

$$\min_{\mathbf{u}_\Delta, \xi_\Delta} \int_0^{t_f} (-P(t) + \Pi(t)) dt \quad (28a)$$

$$\text{subject to: Eqs. (21)–(27)} \quad (28b)$$

which will yield the average power $\bar{P}^* = \int_0^{t_f} P(t) dt / t_f$ needed in Eq. (15). It can be observed that Problem (28) has only quadratic objective function terms and linear constraints; therefore, can be classified as a LQDO problem (see Sec. 1.4).

5 RESULTS

In this section, we describe the results of an LCOE-focused CCD study using the IEA-15 turbine [12] supported by a floating semisubmersible platform [48]. The values for the CCD problem parameters defined in Sec. 4.2 are given in Table 1. Here, we consider six design load cases (DLCs) based on the input wind speed trajectories shown in Fig. 8. The average power values are combined using Eq. (15), with the weights (in days):

$$\tau = [23.0 \ 92.2 \ 115.3 \ 54.0 \ 46.1 \ 34.6] \quad (29)$$

which corresponds to an average wind speed of 13.4 [m/s], and the wind distribution is approximately a Weibull distribution.

The LQDO optimal control problems based on Problem (28) are solved using DTQP, an open-source Matlab-based toolbox using the direct transcription (DT) method and quadratic programming [9, 54]. Each problem was discretized using 2000 mesh points, with an observed relative objective function error bound

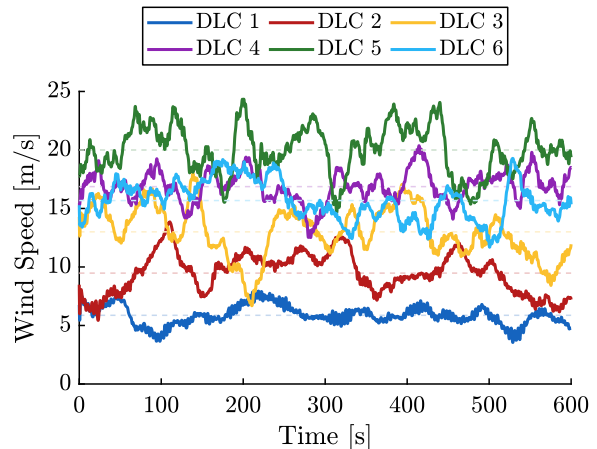


FIGURE 8: Design load cases considered based on an input wind speed trajectory.

of approximately 10^{-4} .

A single critical plant design variable was considered as this time, namely the platform's mass. A sensitivity approach was used to explore how the plant design decisions impact the system cost and performance. More interpolated mass values were added near the lower bound of m_r . In order to understand the impact of platform mass on the system stability, power production, and subsequently the LCOE, several constraint bounds on the platform pitch tilt Θ_p were explored. More specifically, Θ_p was constrained to four different values between 3–6°. Although no wave/current forces are included as disturbances at this time, these different constraint values on Θ_p will roughly indicate performance in more dynamic wave and current conditions.

Overall, there were $32 \times 6 \times 4 = 768$ inner-loop control subproblems solved for each combination of mass, DLC, and $\Theta_{p,\max}$. The computational cost was 37 minutes on a desktop workstation with an AMD 3970X CPU, 128 GB DDR4 2666 MHz RAM, Matlab 2021a update 1, and Windows 10 build 17763.1790. The code for inner loop studies mentioned in the previous sections is available at Ref. [54].

5.1 Results for a Single Control Subproblem

Figure 9 summarizes the optimal control results for 1 of the 264 problems with $m_r = 0.7$, DLC 6, and $\Theta_p \leq 4^\circ$. The optimal trajectories for the generator speed and platform pitch are in Fig. 9a. We see that the constraint $\Theta_p \leq 4^\circ$ and others in Table 1 are satisfied. DLC 6 is in the rated-power region, so we might expect pitch control to be active and the generator torque to be held roughly constant in Fig. 9b [26]. However, to satisfy the platform pitch constraints, we see that the generator speed does need to decrease when the pitch constraint becomes active.

To better understand the optimal control results in other operating regions, Fig. 10 was constructed to show the behavior

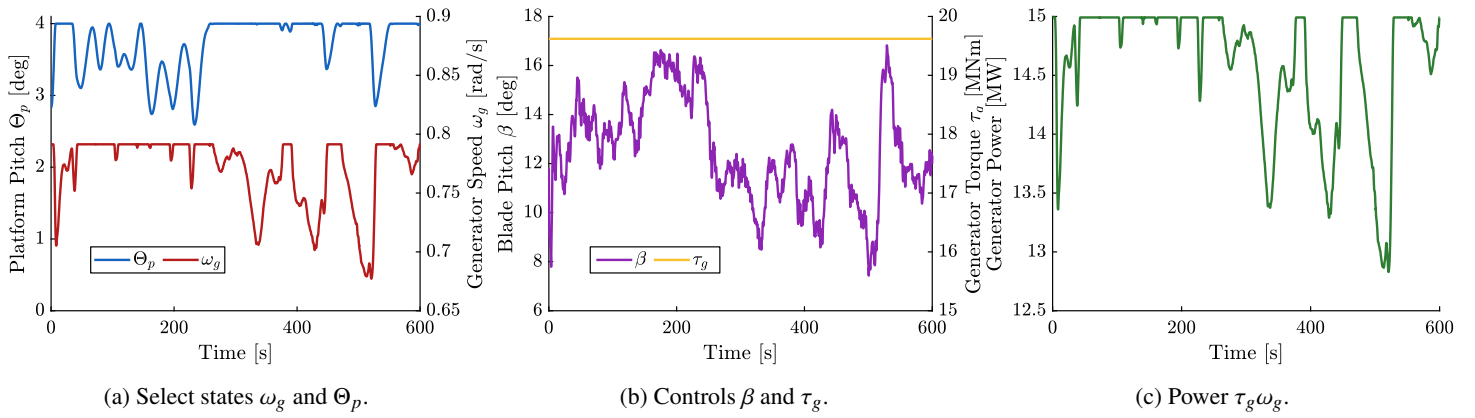


FIGURE 9: Optimal control results with $m_r = 0.7$, DLC 6, and $\Theta_p \leq 4^\circ$.

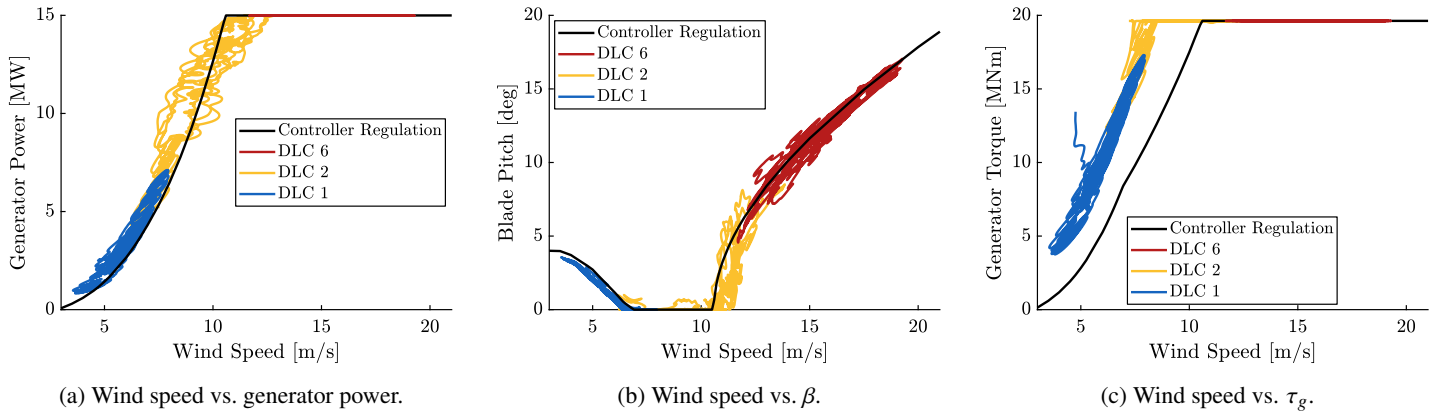


FIGURE 10: Select optimal control results using LPV model vs. controller regulation curves with $m_r = 1$ and $\Theta_p \leq 6^\circ$.

with nominal mass $m_r = 1$ and the largest pitch constraint value $\Theta_p \leq 6^\circ$. We see in Figs. 10b and 10c that the results generally follow the expected trends when compared to the controller regulation from Fig. 2. Overall, the optimization-based approach seems to favor larger torque values and slower speeds than the regulation curves. The results from the DLCs in the below-rated and transition regions are encouraging, as a combination of torque and pitch control is utilized. In some regions, the pitch control is active while torque is held constant and vice versa. Therefore, the optimizer identifies results for all regions in agreement with traditional wind turbine controls. Overall, these results, in combination with the model validation in Sec. 3, demonstrate the validity of the considered LPV models in FOWT open-loop control studies.

5.2 Average Output Power vs. Platform Mass

In Fig. 11, the trends between the average power $\bar{P}_6^*(m_r)$ for DLC 6 are shown for the four tested values of $\Theta_{p,\max}$. The primary method used to control the platform pitch and ensure system stability is the blade pitch β , but β is also tightly coupled to the

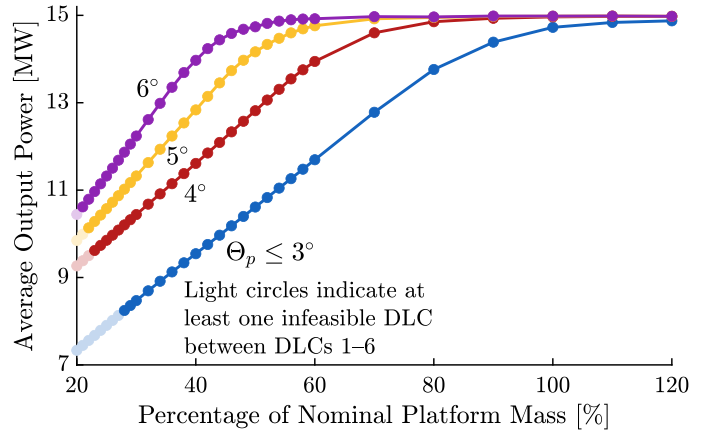


FIGURE 11: Average output power for DLC 6 vs. platform mass.

generator speed. To satisfy smaller, more challenging values of $\Theta_{p,\max}$, the optimal control solution has higher values of blade pitch, sacrificing generator speed. Thus, for these more challeng-

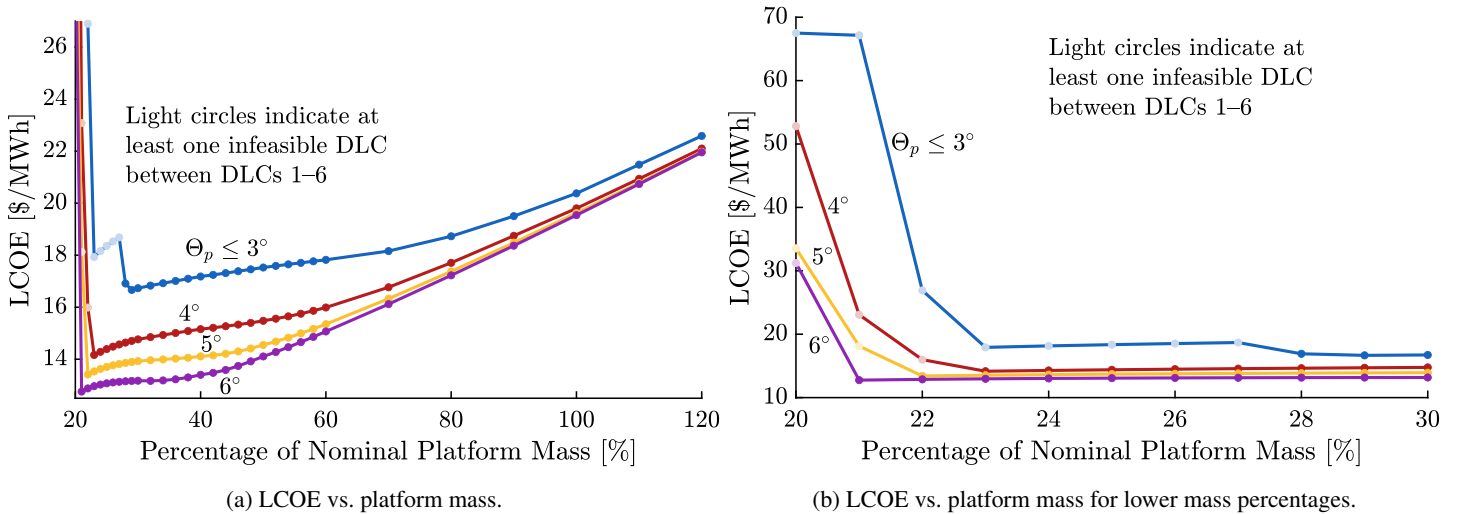


FIGURE 12: LCOE vs. platform mass.

ing constraint values, the power produced is lower on average.

Additionally, the platform mass has a significant effect on the average power production. We see that heavier platforms satisfy the stability constraints with little to no compromise on power generation (i.e., average power is nearly at 15 MW). In comparison, lighter platforms have to sacrifice power generation. Furthermore, in Fig. 11 several points are marked in a lighter shade to indicate that at least one infeasible DLC was identified, i.e., under the constraints imposed in the control subproblem and with the given platform mass, no feasible solution was found. Two trends are observed for these infeasible cases; they happen predominantly for platforms with lower masses and DLCs in the transition region, e.g., DLCs 2 and 3 from Fig. 8. As mentioned previously, the blade pitch is used to control the platform pitch. For platforms with lower masses, the pitch control needs to be close to or at its maximum value to satisfy the tighter platform pitch constraints. For the infeasible cases, the maximum allowable pitch value is not sufficient to satisfy the constraints.

5.3 LCOE vs. Platform Mass

Now, combining the DLCs using the weighting scheme in Eq. (15), we can determine the total energy output. In addition, utilizing the total cost model from Sec. 4.1, LCOE can be estimated. These estimates of LCOE have been calculated for $n = 30$ years with a $r = 7\%$ discount rate. It is important to emphasize that this estimate of LCOE only considers the capital cost of the turbine and platform components and maintenance cost. Other “balance of system” costs [50] are not considered for this study as we are only looking at a single turbine. As mentioned previously, some values of the constraints are infeasible, and the infeasible results are included with zero generated energy. The summarized LCOE results are shown in Fig. 12.

From these results, we see that the optimal value for LCOE depends on the stability constraint; for large values of $\Theta_{p,max}$, the optimal mass decreases. This is because as the platform mass increases, the capital cost increases. But, as indicated in Fig. 11, lower mass values can still result in nearly maximum average power production. Therefore, there is some optimal mass point where the conflicting decisions of increasing energy production are balanced with increasing platform capital costs.

For the considered reference IEA-15 turbine described in Refs. [12, 48], Θ_p was constrained to 6° using the nominal platform mass. While keeping the other plant parameters constant, we see that the lowest LCOE, in this case, is achieved using 40% of the nominal platform mass. However, this result is subject to modeling assumptions, optimal control operation, and lack of safety factors, but it can still help guide the final design. Additionally, the hydrodynamic and hydrostatic stability of the different platforms has not been evaluated in this study. These investigations will also limit the bounds on the platform mass and impact the final design.

6 CONCLUSION

In this work, we discussed the use of linear parameter-varying (LPV) models for control co-design (CCD) of floating offshore wind turbines (FOWTs). High-fidelity models of FOWTs are described by highly complex and nonlinear models. Unfortunately, these models are often too costly to use in early-stage system design and evaluation. Using linearized models based on these nonlinear systems is a popular method to offset the computational costs involved. Here, we describe a class of linear parameter-varying (LPV) models that realize more accurate predictions of a system’s dynamic behavior over a large range of

operating points and are shown to be useful for early-stage CCD studies of FOWTs.

The specific FOWT system considered was the IEA-15 reference turbine [12] on a semisubmersible platform [48]. The LPV models based on the wind speed parameter showed good general agreement in both nonlinear simulation comparisons and general optimal control trends. The primary study investigated the system's dynamic stability, power production, and ultimately the levelized cost of energy (LCOE). The single plant decision in this study was the platform's mass, and the optimal LCOE results indicated that the platform mass could be reduced to 30–60% of its nominal value and still satisfy the platform pitch constraints. However, several additional factors should be investigated before making a specific recommendation.

It remains future work to incorporate more detailed and sophisticated outer-loop plant design optimization, including the impact of plant decisions like tower hub height and blade length on platform stability and power production in the context of the LCOE. With additional plant decisions, the LCOE calculation should also be amended to reflect the omitted factors. Additionally, we hope to study the effect of wave and current excitations. Finally, in order to address the realizability of the open-loop optimal control solutions, work is needed to realize robust, implementable control systems, which may be informed by the optimal operation identified in this study [2, 42].

ACKNOWLEDGMENT

The information, data, or work presented herein was funded in part by the Advanced Research Projects Agency-Energy (ARPA-E), U.S. Department of Energy, under Award Number DE-AC36-08GO28308. The authors would like to thank Alan Wright, Garrett Barter, and Dan Zalkind from NREL for their feedback and suggestions.

REFERENCES

- [1] Garcia-Sanz, M., 2019. "Control co-design: An engineering game changer". *Advanced Control for Applications: Engineering and Industrial Systems*, **1**(1), Oct., p. e18. doi: [10.1002/adc2.18](https://doi.org/10.1002/adc2.18)
- [2] Jonkman, J., Wright, A., Barter, G., Hall, M., Allison, J. T., and Herber, D. R., 2021. "Functional requirements for the WEIS toolset to enable controls co-design of floating offshore wind turbines". In International Offshore Wind Technical Conference, no. IOWTC2020-3533.
- [3] Sandner, F., Schlipf, D., Matha, D., and Cheng, P. W., 2014. "Integrated optimization of floating wind turbine systems". In International Conference on Ocean, Offshore and Arctic Engineering. doi: [10.1115/omae2014-24244](https://doi.org/10.1115/omae2014-24244)
- [4] Barter, G. E., Robertson, A., and Musial, W., 2020. "A systems engineering vision for floating offshore wind cost optimization". *Renew. Energy Focus*, **34**, Sept., pp. 1–16. doi: [10.1016/j.ref.2020.03.002](https://doi.org/10.1016/j.ref.2020.03.002)
- [5] Hegseth, J. M., Bachynski, E. E., and Martins, J. R. R. A., 2020. "Design optimization of spar floating wind turbines considering different control strategies". *J. Phys.: Conf. Ser.*, **1669**, Oct., p. 012010. doi: [10.1088/1742-6596/1669/1/012010](https://doi.org/10.1088/1742-6596/1669/1/012010)
- [6] Fleming, P. A., Pineda, I., Rossetti, M., Wright, A. D., and Arora, D., 2014. "Evaluating methods for control of an offshore floating turbine". In International Conference on Ocean, Offshore and Arctic Engineering. doi: [10.1115/omae2014-24107](https://doi.org/10.1115/omae2014-24107)
- [7] Allison, J. T., Guo, T., and Han, Z., 2014. "Co-design of an active suspension using simultaneous dynamic optimization". *J. Mech. Design*, **136**(8), June. doi: [10.1115/1.4027335](https://doi.org/10.1115/1.4027335)
- [8] Deshmukh, A. P., and Allison, J. T., 2015. "Multidisciplinary dynamic optimization of horizontal axis wind turbine design". *Struct. Multidiscip. Optim.*, **53**(1), Aug., pp. 15–27. doi: [10.1007/s00158-015-1308-y](https://doi.org/10.1007/s00158-015-1308-y)
- [9] Herber, D. R., 2017. "Advances in combined architecture, plant, and control design". Ph.D. Dissertation, University of Illinois at Urbana-Champaign, Urbana, IL, USA, Dec.
- [10] Fathy, H. K., Papalambros, P. Y., Ulsoy, A. G., and Hrovat, D., 2003. "Nested plant/controller optimization with application to combined passive/active automotive suspensions". In American Control Conference. doi: [10.1109/ACC.2003.1244053](https://doi.org/10.1109/ACC.2003.1244053)
- [11] Nash, A. L., and Jain, N., 2020. "Combined plant and control co-design for robust disturbance rejection in thermal-fluid systems". *IEEE Trans. Control Syst. Technol.*, **28**(6), pp. 2532–2539. doi: [10.1109/tcst.2019.2931493](https://doi.org/10.1109/tcst.2019.2931493)
- [12] Gaertner, E., Rinker, J., Sethuraman, L., Zahle, F., Anderson, B., Barter, G. E., Abbas, N. J., Meng, F., Bortolotti, P., Skrzypinski, W., Scott, G. N., Feil, R., Bredmose, H., Dykes, K., Shields, M., Allen, C., and Viselli, A., 2020. IEA wind TCP task 37: definition of the IEA 15-megawatt offshore reference wind turbine. Tech. rep., Mar. doi: [10.2172/1603478](https://doi.org/10.2172/1603478)
- [13] Zalkind, D. S., Ananda, G. K., Chetan, M., Martin, D. P., Bay, C. J., Johnson, K. E., Loth, E., Griffith, D. T., Selig, M. S., and Pao, L. Y., 2019. "System-level design studies for large rotors". *Wind Energy Sci.*, **4**(4), Nov., pp. 595–618. doi: [10.5194/wes-4-595-2019](https://doi.org/10.5194/wes-4-595-2019)
- [14] Coe, R. G., Bacelli, G., Olson, S., Neary, V. S., and Topper, M. B. R., 2020. "Initial conceptual demonstration of control co-design for WEC optimization". *J. Ocean Eng. Mar. Energy*, **6**(4), Nov., pp. 441–449. doi: [10.1007/s40722-020-00181-9](https://doi.org/10.1007/s40722-020-00181-9)
- [15] Herber, D. R., 2014. "Dynamic system design optimization of wave energy converters utilizing direct transcription". M.S. Thesis, University of Illinois at Urbana-Champaign, Urbana, IL, USA, May.
- [16] Brodrick, P. G., Kang, C. A., Brandt, A. R., and Durlofsky, L. J., 2015. "Optimization of carbon-capture-enabled coal-gas-solar power generation". *Energy*, **79**, Jan., pp. 149–162. doi: [10.1016/j.energy.2014.11.003](https://doi.org/10.1016/j.energy.2014.11.003)
- [17] Gros, S., 2013. "An economic NMPC formulation for wind turbine control". In IEEE Conference on Decision and Control. doi: [10.1109/cdc.2013.6760013](https://doi.org/10.1109/cdc.2013.6760013)
- [18] Ghigo, A., Cottura, L., Caradonna, R., Bracco, G., and Mattiazzo, G., 2020. "Platform optimization and cost analysis in a floating offshore wind farm". *J. Mar. Sci. Eng.*, **8**(11), Oct., p. 835. doi: [10.3390/jmse8110835](https://doi.org/10.3390/jmse8110835)
- [19] Kikuchi, Y., and Ishihara, T., 2019. "Upscaling and levelized cost of energy for offshore wind turbines supported by semi-submersible floating platforms". *J. Phys.: Conf. Ser.*, **1356**, Oct., p. 012033. doi: [10.1088/1742-6596/1356/1/012033](https://doi.org/10.1088/1742-6596/1356/1/012033)
- [20] Musial, W. D., Beiter, P. C., Spitsen, P., Nunemaker, J., and Gevorgian, V., 2019. 2018 offshore wind technologies market report. Tech. rep., Sept. doi: <https://doi.org/10.2172/1572771>
- [21] Ennis, B. L., and Griffith, D. T., 2018. System levelized cost of energy analysis for floating offshore vertical-axis wind turbines. Tech. rep., Aug. doi: [10.2172/1466530](https://doi.org/10.2172/1466530)
- [22] Beiter, P., Musial, W., Smith, A., Kilcher, L., Damiani, R., Maness, M., Sirmivas, S., Stehly, T., Gevorgian, V., Mooney, M., and Scott, G., 2016. A spatial-economic cost-reduction pathway analysis for U.S. offshore wind energy development from 2015–2030. Tech. rep., Sept. doi: [10.2172/1324526](https://doi.org/10.2172/1324526)
- [23] Johannessen, M., 2018. "Concept study and design of floating off-

- shore wind turbine support structure”. Degree Project, KTH Royal Institute of Technology.
- [24] Hopstad, A. L. H., Argyriadis, K., Manjock, A., Goldsmith, J., and Ronold, K. O., 2018. “DNV GL standard for floating wind turbines”. In ASME International Offshore Wind Technical Conference. doi: [10.1115/iowtc2018-1035](https://doi.org/10.1115/iowtc2018-1035)
- [25] DNV, 2013. Design of offshore wind turbine structures. Tech. rep., June.
- [26] Pao, L. Y., and Johnson, K. E., 2009. “A tutorial on the dynamics and control of wind turbines and wind farms”. In American Control Conference. doi: [10.1109/acc.2009.5160195](https://doi.org/10.1109/acc.2009.5160195)
- [27] Moriarty, P. J., and Butterfield, S. B., 2009. “Wind turbine modeling overview for control engineers”. In American Control Conference. doi: [10.1109/acc.2009.5160521](https://doi.org/10.1109/acc.2009.5160521)
- [28] Lemmer, F., 2018. Low-order modeling, controller design and optimization of floating offshore wind turbines. doi: [10.18419/OPUS-10526](https://doi.org/10.18419/OPUS-10526)
- [29] Lemmer, F., Yu, W., Luhmann, B., Schlipf, D., and Cheng, P. W., 2020. “Multibody modeling for concept-level floating offshore wind turbine design”. *Multibody Syst. Dyn.*, **49**(2), Feb., pp. 203–236. doi: [10.1007/s11044-020-09729-x](https://doi.org/10.1007/s11044-020-09729-x)
- [30] Smilden, E., Horn, J.-T. H., Sørensen, A. J., and Amdahl, J., 2016. “Reduced order model for control applications in offshore wind turbines”. *IFAC-PapersOnLine*, **49**(23), pp. 386–393. doi: [10.1016/j.ifacol.2016.10.435](https://doi.org/10.1016/j.ifacol.2016.10.435)
- [31] Pereira, H., Cupertino, A., Teodorescu, R., and Silva, S., 2014. “High performance reduced order models for wind turbines with full-scale converters applied on grid interconnection studies”. *Energies*, **7**(11), Nov., pp. 7694–7716. doi: [10.3390/en7117694](https://doi.org/10.3390/en7117694)
- [32] Jonkman, J. M., and Jonkman, B. J., 2016. “FAST modularization framework for wind turbine simulation: full-system linearization”. *J. Phys.: Conf. Ser.*, **753**, Sept., p. 082010. doi: [10.1088/1742-6596/753/8/082010](https://doi.org/10.1088/1742-6596/753/8/082010)
- [33] Jonkman, J., Wright, A. D., Hayman, G., and Robertson, A. N., 2018. Full-system linearization for floating offshore wind turbines in OpenFAST: Preprint. Tech. rep., Dec. doi: [10.2172/1489323](https://doi.org/10.2172/1489323)
- [34] van Wingerden, J. W., Houtzager, I., Felici, F., and Verhaegen, M., 2009. “Closed-loop identification of the time-varying dynamics of variable-speed wind turbines”. *Int. J. Robust Nonlinear Control*, **19**(1), Jan., pp. 4–21. doi: [10.1002/rnc.1320](https://doi.org/10.1002/rnc.1320)
- [35] Bianchi, F., Mantz, R., and Christiansen, C., 2005. “Gain scheduling control of variable-speed wind energy conversion systems using quasi-LPV models”. *Control Eng. Pract.*, **13**(2), Feb., pp. 247–255. doi: [10.1016/j.conengprac.2004.03.006](https://doi.org/10.1016/j.conengprac.2004.03.006)
- [36] Lescher, F., Zhao, J. Y., and Martinez, A., 2006. “Multiobjective H_2/H_∞ control of a pitch regulated wind turbine for mechanical load reduction”. *Renewable Energy and Power Quality Journal*, **1**(04), Apr., pp. 100–105. doi: [10.24084/REPQJ04.248](https://doi.org/10.24084/REPQJ04.248)
- [37] Herber, D. R., and Allison, J. T., 2018. “Nested and simultaneous solution strategies for general combined plant and control design problems”. *J. Mech. Design*, **141**(1), Oct. doi: [10.1115/1.4040705](https://doi.org/10.1115/1.4040705)
- [38] Sundararajan, A. K., and Herber, D. R., 2021. “Towards a fair comparison between the nested and simultaneous control co-design methods using an active suspension case study”. In American Control Conference.
- [39] Azad, S., and Alexander-Ramos, M. J., 2019. “Reliability-based MDSO for co-design of stochastic dynamic systems”. In International Mechanical Engineering Congress and Exposition. doi: [10.1115/IMECE2019-10632](https://doi.org/10.1115/IMECE2019-10632)
- [40] Herber, D. R., and Allison, J. T., 2019. “A problem class with combined architecture, plant, and control design applied to vehicle suspensions”. *J. Mech. Design*, **141**(10), May. doi: [10.1115/1.4043312](https://doi.org/10.1115/1.4043312)
- [41] Herber, D. R., and Sundararajan, A. K., 2020. “On the uses of linear-quadratic methods in solving nonlinear dynamic optimization problems with direct transcription”. In ASME International Mechanical Engineering Congress & Exposition, no. IMECE2020-23885.
- [42] Deshmukh, A. P., Herber, D. R., and Allison, J. T., 2015. “Bridging the gap between open-loop and closed-loop control in co-design: A framework for complete optimal plant and control architecture design”. In American Control Conference, pp. 4916–4922. doi: [10.1109/ACC.2015.7172104](https://doi.org/10.1109/ACC.2015.7172104)
- [43] Deshmukh, A. P., and Allison, J. T., 2017. “Design of dynamic systems using surrogate models of derivative functions”. *J. Mech. Design*, **139**(10), Aug. doi: [10.1115/1.4037407](https://doi.org/10.1115/1.4037407)
- [44] WEIS. [Online, version 52d0b88]. url: <https://github.com/WISDEM/WEIS>
- [45] OpenFAST. [Online]. url: <https://github.com/OpenFAST/openfast>
- [46] Martin, D. P., Johnson, K. E., Zalkind, D. S., and Pao, L. Y., 2017. “LPV-based torque control for an extreme-scale morphing wind turbine rotor”. In American Control Conference, IEEE. doi: [10.23919/ACC.2017.7963146](https://doi.org/10.23919/ACC.2017.7963146)
- [47] IEA-15-240-RWT. [Online, version 9aa6ce4]. url: <https://github.com/IEAWindTask37/IEA-15-240-RWT>
- [48] Allen, C., Viscelli, A., Dagher, H., Goupee, A., Gaertner, E., Abbas, N., Hall, M., and Barter, G., 2020. Definition of the UMaine VoltturnUS-S reference platform developed for the IEA wind 15-megawatt offshore reference wind turbine. Tech. rep., July. doi: [10.2172/1660012](https://doi.org/10.2172/1660012)
- [49] WISDEM. [Online, version 52d0b88]. url: <https://github.com/WISDEM/WISDEM>
- [50] Fingersh, L., Hand, M., and Laxson, A., 2006. Wind turbine design cost and scaling model. Tech. rep., Dec. doi: [10.2172/897434](https://doi.org/10.2172/897434)
- [51] Malcolm, D. J., and Hansen, A. C., 2006. WindPACT turbine rotor design study: June 2000–June 2002 (revised). Tech. rep., Apr. doi: [10.2172/15000964](https://doi.org/10.2172/15000964)
- [52] Maples, B., Hand, M., and Musial, W., 2010. Comparative assessment of direct drive high temperature superconducting generators in multi-megawatt class wind turbines. Tech. rep., Oct. doi: [10.2172/991560](https://doi.org/10.2172/991560)
- [53] Betts, J. T., 2010. *Practical methods for optimal control and estimation using nonlinear programming*. Society for Industrial and Applied Mathematics, Jan. doi: [10.1137/1.9780898718577](https://doi.org/10.1137/1.9780898718577)
- [54] The DTQP project. [Online, version 0069e01]. url: <https://github.com/danielrherber/dt-qp-project>